Polymer Based Highly Parallel Nanoscopic Sensors for Rapid Detection of Chemicals and Biological Threats

Final Technical Report

NRL Contract No. N00173-05-C-6022

For the work performed July 25, 2005 – July 24, 2007

Dr. Ryan Giedd, Principle Investigator
Mr. Matt Curry, Co-Principle Investigator
Dr. Xuliang Han, PI of Brewer Science, Inc. Subcontract

Center for Applied Science & Engineering
Missouri State University
901 South National Avenue
Springfield, Missouri 65897

REPORT DOCUMENTATION PAGE

Form Approved
OMB No. 0704-0188

1. REPORT DATE (DD-MM-YYYY)	2. REPORT DATE	3. DATES COVERED: *(From – To)*
9/18/2007	Final Technical	6/21/2003-7/10/2006

4. TITLE AND SUBTITLE

Polymer Based Highly Parallel Nanoscopic Sensors for Rapid Detection of Chemical and Biological Threats

5a. CONTRACT NUMBER
N00173-05-C-6022

5b. GRANT NUMBER
n/a

5c. PROGRAM ELEMENT NUMBER
n/a

6. AUTHOR(S)

Giedd, Ryan
Han, Xuliang
Curry, Matt

5d. PROJECT NUMBER
56-9112-05

5e. TASK NUMBER
n/a

5f. WORK UNIT NUMBER
n/a

7. PERFORMING ORGANIZATION NAME(S) AND ADDRESS(ES)
Missouri State University
901 South National Avenue
Springfield, MO 65897

8. PERFORMING ORGANIZATION REPORT NUMBER
n/a

9. SPONSORING/MONITORING AGENCY NAME(S) AND ADDRESS(ES)
Contracting Officer
Naval Research Laboratory - SSC
Department of the Navy
Stennis Space CTR. ,MS 39529-5004

10. SPONSOR/MONITOR'S ACRONYM(S)
NRL

AGENCY REPORT NUMBER

12. DISTRIBUTION AVAILABILITY STATEMENT
Approved for Public Release, distribution is Unlimited.

13. SUPPLEMENTARY NOTES

14. ABSTRACT

Raw carbon nanotubes (CNTs) contain a wide range of impurities from the growth process. At Brewer Science an effective post-growth purification procedure was developed to reduce the amount of impurities, and several characterization techniques were developed and validated.

15. SUBJECT TERMS

16. SECURITY CLASSIFICATION OF:			17. LIMITATION OF ABSTRACT	18. NUMBER OF PAGES	19a. NAME OF RESPONSIBLE PERSON
a. REPORT	b. ABSTRACT	C. THIS PAGE			Ryan Giedd, Ph.D.
U	U	U	SAR	28	**20b. TELEPHONE NUMBER (include area code)** 417-836-5279

ABSTRACT

Raw carbon nanotubes (CNTs) contain a wide range of impurities from the growth process. At Brewer Science an effective post-growth purification procedure was developed to reduce the amount of impurities, and several characterization techniques were developed and validated.

CONTENT

FIGURES & TABLES

Page No.

SUMMARY

CNTs need to be free of any impurity so that their unique properties can be utilized for any electronic-grade applications. The impurities that can be found in raw CNTs include the remnants of the transition-metal catalysts that are required for the synthesis of CNTs and various carbonaceous materials rather than CNTs. In this project a number of analytical methods were developed to determine the impurities in the raw CNTs from various vendors. An effective post-growth purification procedure was developed to reduce the amount of impurities, and several characterization techniques, including optical density, dilution curve, trace metals, wafer electrical testing, filter disc electrical testing, and Raman spectroscopy, were developed and validated. Also investigated in this project were raw material source impact and waste stream.

INTRODUCTION

Raw CNTs are very fluffy soot, and thus it is very difficult to directly handle them in any device fabrication process. Furthermore, there is always a great amount of impurities in raw CNTs, including metallic particles from the catalysts and carbonaceous materials from the chemical reaction by-products. The concentration of metallic impurities is typically 30-50%, whereas the tolerance of metallic particles in a device is extremely tight, because even a small amount can cause many serious problems, such as electrical short, charge accumulation, and threshold shift. Amorphous carbon (α-C) is a major carbonaceous impurity, which usually covers the sidewalls of CNTs, forming huge barriers at the interfaces among CNTs. Such barriers can significantly restrict the tube-to-tube carrier transport. Therefore, purifying CNTs and dispersing the purified CNTs into a benign solvent system become a crucial step for utilizing the unique properties of CNTs in various applications.

METHODS, ASSUMPTIONS, & PROCEDURES

Screening of Raw CNTs

Several synthetic approaches, such as electrical arc discharge, laser ablation, flame combustion, and chemical vapor deposition (CVD), have been developed to grow CNTs. At this stage, however, all raw materials, or so-called as-produced materials, contain a significant amount of impurities, including metallic particles from the catalysts and carbonaceous impurities from the chemical reaction by-products. Employing appropriate methods to characterize the impurities in raw CNTs is a critical part of the purification effort. At Brewer Science a series of techniques have been developed and validated for screening raw CNTs.

Metallic Impurities

The metallic particles in the raw CNTs are mainly from the transition-metal catalysts that must be used in the synthesis process. The presence of metallic particles in a raw CNT sample can be detected and the types of these metals can be identified through the X-ray diffraction (XRD) measurement. XRD is a technique in crystallography in which

the patterns produced by the diffraction of X-rays through the closely spaced lattice of the atoms in a crystal are recorded and then analyzed to reveal the nature of the substance.

The concentration of the metallic particles in a raw CNT sample can be determined through the thermogravimetric analysis (TGA). TGA is an analytical technique widely used to study the thermal stability of a substance in a controlled atmosphere and its fraction of volatile components by monitoring the weight change that occurs as this substance is heated. For a raw CNT sample, the weight change in the regular atmosphere is typically a superposition of the weight loss due to the oxidation of carbon into gaseous carbon dioxide and the weight gain due to the oxidation of metal into solid oxide. In the standard TGA, the airflow rate is regulated at 100 sccm, and the raw CNT sample is heated from room temperature up to 800 ^{o}C at a ramp rate of 5 ^{o}C/min.

Another effective method to measure the concentrations of various metals is to conduct an ICP-MS (Inductively Coupled Plasma Mass Spectrometry) or an AA (Atomic Absorption) measurement after the solid CNT soot has been completely digested in an acid solution. At Brewer Science the following procedure has been developed:

1. Soaking CNT soot with concentrated HNO_3 at 100 ^{o}C for 50 hours
2. Performing periodic ultrasonication
3. Adjusting concentration with deionized (DI) water
4. Conducting ICP-MS or AA measurement

At the end of the digestion process, the obtained liquid sample does not contain any solid particle, which ensures the accuracy of the following ICP-MS or AA measurement. The results obtained by using this method have been confirmed to be consistent with those obtained through the TGA procedure. Moreover, the use of ICP-MS can detect the presence of a trace metal at the ppb (part per billion) level.

Carbonaceous Impurities

The carbonaceous impurities in raw CNTs include α-C, graphitic carbon, and various non-tubular fullerenes. Because CNTs possess a much higher structural aspect ratio than such carbonaceous impurities, HRTEM (High-Resolution Transmission Electron Microscopy) images can be used to evaluate the purity in a graphical manner. However, such estimation cannot be deemed conclusive since the distribution of carbonaceous impurities is highly inhomogeneous at such a nanoscopic scale. Although different forms of carbon exhibit separate on-set oxidation temperatures in a TGA derivative curve, a quantitative fraction analysis is always interfered by the catalytic oxidation effect from the metallic particles. Therefore, how to quantitatively characterize the carbonaceous impurities in a bulk raw CNT sample has been a great challenge. At Brewer Science a practical technique has been developed based on the solution-phase spectrophotometry. The raw CNTs used for this study were commercially obtained from Carbon Nanotechnologies, Inc. (CNI), which were synthesized by the HiPco (High Pressure CO) process. Iron particles with an average diameter of ~ 2 nm were detected in the powder through the XRD measurement, and the concentration of iron was determined to be ~ 30 wt% through the standard TGA. It is well known that individual CNTs can be suspended in an aqueous medium by using various surfactants. The surfactant solution used for this

study was prepared by dissolving sodium dodecyl sulfate (SDS) in deionized (DI) water at a concentration of 1 wt%. For the optical absorption spectrum study covering an even wider infrared region, heavy water (D_2O) was used instead of DI water. For this study, the CNT suspension was obtained in the following manner. First, approximately 10 mg raw HiPco CNTs were dispersed into 100 mL SDS aqueous solution in a quartz flask by performing a sonication for 30 minutes in a water bath cooled at 5 ^{o}C. The average ultrasonic power density measured in the proximity of the quartz flask inside the water bath was ~ 50 W/cm^2. In order to sediment the remaining particles, which would interfere with the following optical absorption spectrum measurement, the sonicated CNT dispersion was kept at room temperature for 24 hours. Finally, a non-scattering CNT suspension was obtained by decanting the upper ~ 50% portion of the stabilized dispersion. By following the same experimental procedure, a non-scattering α-C suspension was prepared as well for conducting the comparative study.

Production of Electronic-Grade CNT Solutions

Functionalization

Functionalization consists of a high-temperature concentrated nitric acid reflux, followed by partial neutralization with ammonium hydroxide. The reactor was originally designed based on the previous experience with 1 to 100 liter glass reactors. Figure 1 shows the assembled reactor, which consists of a 2-piece reactor vessel (1), a heat source (2), a condenser (3), and an agitator (4). The system also includes a temperature control system, which consists of a reaction temperature sensor (5), a heat source temperature sensor (6), and a condenser outlet temperature (7).

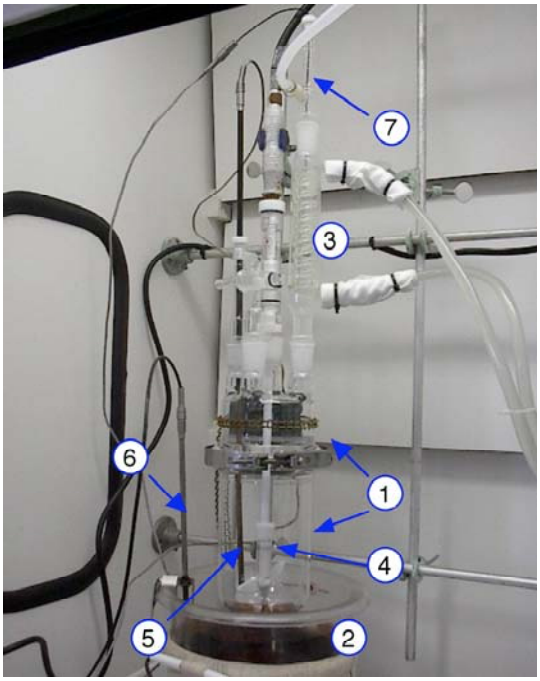

Figure 1. Assembled functionalization reactor

The original design was modified only slightly through the course of the project. In the final design, the heat source was changed from an oil bath to a heating mantle. The oil bath required the assembly to be suspended in the oil by using external clamps. The clamps were attached at the union of the reactor head and base. In comparison, the mantle provided a much sturdier base for the system and made the alignment of the agitator easier. Also, the oil bath was made of glass, which could be accidentally broken and potentially spill hot oil. This change in heat source was the only significant change to the original reactor design.

Removal of Metals, Salts, α-C, and Small Particles

Cross-flow filtration, which is sometimes referred to as dialysis or tangential flow filtration, was utilized to "flush" metal ions, α-C, and other undesirable small particles from the purified CNT solution. Figure 2 shows the schematic of this process. The CNT solution is passed along a membrane that is permeable to the aqueous carrier but blocks passage of CNTs. While the backpressure is driving the solution to pass through the membrane, CNTs are retained on the barrier side of the membrane, and the solution carries metal ions, salts, acid waste, and other small particles away. Fresh and clean carrier solvent is added to replace the volume passed through the membrane (permeate). Flowing of retained material (retentate) tangentially along the membrane prevents the buildup of a filter cake. Ultrasonic waves are used to gently disentangle CNTs during the filtration process.

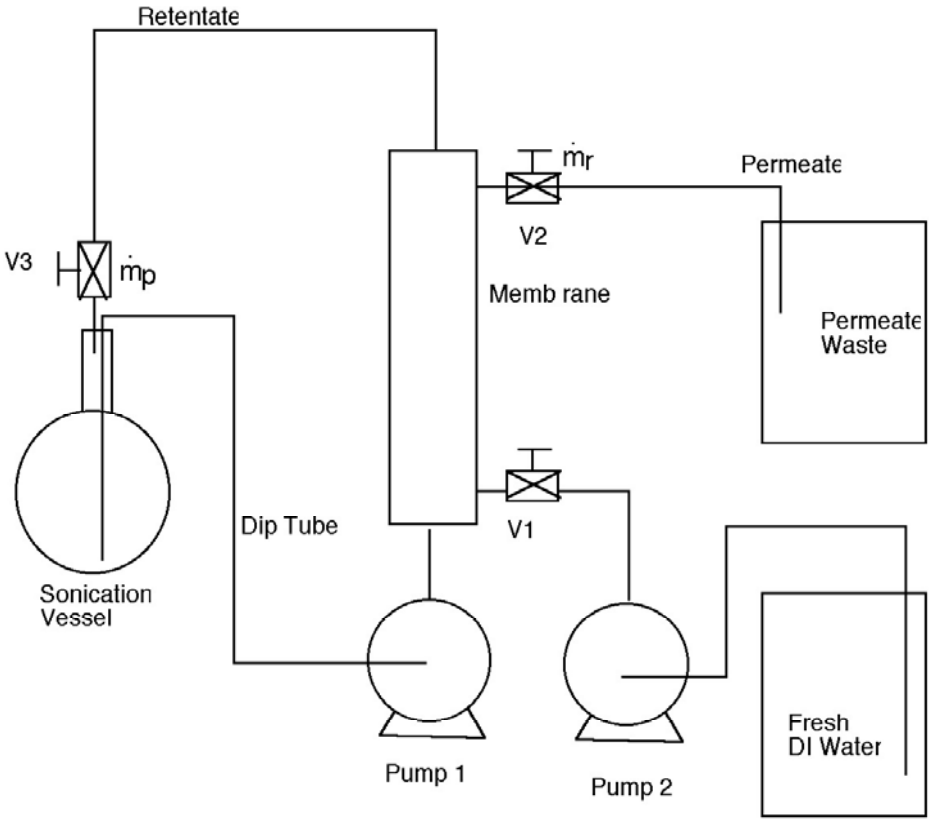

Figure 2. Schematic of cross-flow filtration process

The equipment originally configured for this process is shown in Figure 3, which consists of a filter membrane (1), two pumps (2) (3), a sonication vessel (4), a fresh DI water reservoir (5), a permeate waste container (6), an ultrasonication equipment (7), and a temperature control equipment (8).

Figure 3. Original cross-flow filtration process equipment design

However, it was discovered that the original design was not well suited for the commercial application. The system would be very labor intensive, requiring manual actuation of a number of valves to reconfigure the system between the filtration step and the recovery step. Also, the original design required the operator to change the tubing to reconfigure the filtration pump into a recovery pump. Using this type of pump in the

high-pressure recovery process exceeded the operating pressure of some check valve components, which caused leaks and constant preventive maintenance. Figure 4 shows the redesigned equipment from front and back view, respectively. The new design eliminates manual changes in configuration between the filtration and recovery steps. Electrically activated valves have replaced the manually operated valves, which allows a single switch to open/close valves in the correct configuration for each process operation. Since all components are not manually operated, they can be located in a more convenient location (in this case on the back side), freeing more workspace. The new system adds an additional pump for the recovery process, and thus the filtration pump does not have to serve a second function for which it is not suited, operating in the designed pressure range of the recovery process. This ensures the safety by preventing leaks, reduces preventive maintenance, and increases the efficiency of the recovery process. The final result is a more commercially robust system that can be further automated by the addition of a PLC control unit.

Figure 4. Final cross-flow filtration process equipment design

Removal of large particles

Ultracentrifugation was utilized for the removal of large particles. Both batch and continuous flow ultracentrifugation are available. Batch ultracentrifugation has been demonstrated as an effective technique. However, this process is labor intensive. Continuous flow ultracentrifugation offers more commercial profitability, but it has been proved that it would require batch volumes larger than those produced within the scope of this project.

Characterization of Electronic-Grade CNT Solutions

Optical Density

Optical density (OD) refers to the absorbance at wavelength of 550 nm by the sample. This reading can indicate the concentration of carbon in the solution. Therefore, it can be used to verify the consistency in the concentrations of various samples and to adjust the concentration of a given sample to a specified level.

Dilution Curve

The dilution procedure is to lower the concentration of carbon in the solution from the standard OD to a target OD. To establish this procedure, a series of samples were prepared by adding a series of known amount of DI water to the solution having the standard OD, measuring the OD values of the resulting diluted solutions, and then using an empirical equation to describe the measurement response, finally using this equation to predict the appropriate amount of DI water needed to achieve any desired OD. The dilution curve method is illustrated below in Figure 5.

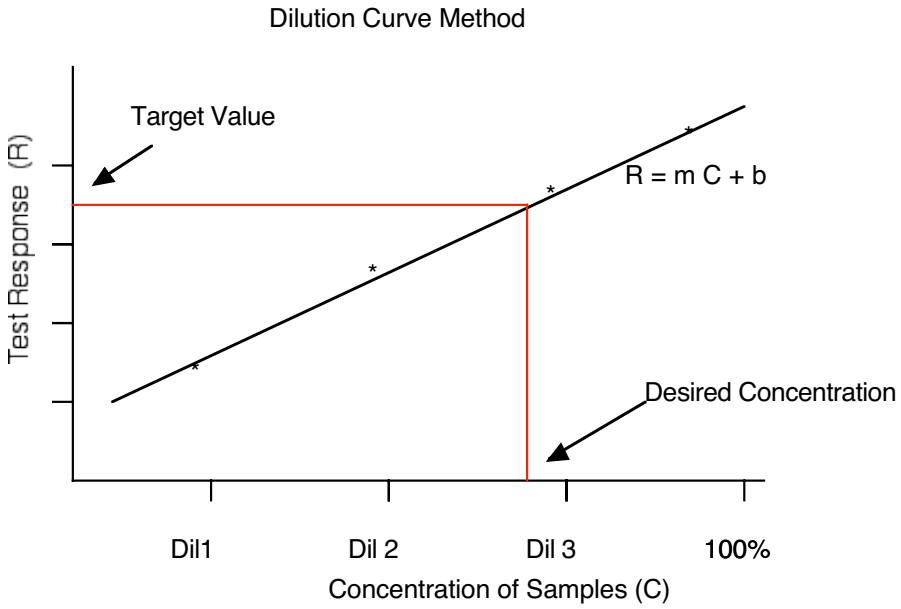

Figure 5. Illustration of dilution curve method

Trace Metals

The ions trapped in the gate oxide layer can degrade the performance of a CMOS device by causing bias shift and instability. Therefore, ion contamination is a critical concern in CMOS manufacturing. Any material involved in a CMOS device fabrication process may be an ion source, and thus our goal is to lower the concentrations of the trace metals in the purified CNT solutions to a level that is in compliance to the widely accepted CMOS industry standard. At Brewer Science ICP-MS was used for measuring the concentrations of the trace metals.

Wafer Electrical Testing

For characterizing the purified CNT solutions, this test consists of spin-coating 4" silicon oxide wafers by using a BSI 100CB spin coater and a BSI 10-10 hotplate, followed by measuring the sheet resistance values of the resulting CNT films. In theory, the CNT films coated under the properly controlled conditions will have the same sheet resistance values if the properties of CNT solutions are identical. Therefore, the effort to produce purified CNT solutions with repeatable properties can be monitored with such a test. In this test, controlling the coating conditions is critical, since the spin-coating process is sensitive to a number of environmental conditions, including temperature, relative humidity, exhaust, air flow over, wafer surface property, solution-casting manner, and spin-coating recipe.

Because the product being developed is water based, the wafer surface property has a great influence on the uniformity of the resulting CNT films. It was discovered that having a hydrophilic wafer surface was critical. When using thermal silicon oxide, which has a hydrophobic surface, an additional surface treatment becomes necessary. It was found that a 1-2 sec dip of the wafers in a diluted HF solution was sufficient to create the required hydrophilic condition. Currently this wafer surface treatment has been implemented at the wafer manufacturing facility, as it has become a component of the purchase specifications for the wafers.

The basic spin-coating process is to first conduct a "dehydration bake" to evaporate any moisture on the wafer surface. This dehydration bake consists of 5 min hotplate baking at 300 °C, followed by a 3 min cooling at room temperature. The spin-coating process itself consists of the following phases: (0) dispensing, (1) smoothing, (2) drying, (3) edge bead removal, (4) deceleration, and (5) stop. The recipe parameters in each phase are listed below in Table 1. During the dispensing phase, 5 mL purified CNT solution is cast manually with an Ependorph pipette, moving along the radial direction starting from the center of the wafer. After the spin-coating recipe is executed, a 2 min hotplate baking at 200 °C follows. After a 3 min cooling at room temperature has elapsed, the next coat can proceed following the above spin-coating procedure and recipe.

Step	0	1	2	3	4	5
Velocity	60	525	76	2000	0	End
Ramp	200	500	500	1000	1000	
Time	20	1	300	8	0	

Table 1. Spin-coating recipe

After forming CNT films on the wafers, the sheet resistance values were measured with a 4-point probe at 9 points across the wafer. The average resistance and uniformity were recorded.

Filter Disc Electrical Testing

A vacuum filtration setup was assembled, as shown in Figure 6. The nominal pore size of the filter disc membrane used for this study is 0.02 μm. With such a small pore size,

the majority of the solid content in the purified CNT solution can be captured by the membrane, as shown in Figure 7. By using this vacuum filtration setup, densely packed CNT films can be formed, as shown in Figure 8. By measuring the weight (m) of the solid collected on the filter disc with a high-precision microbalance, the concentration of the purified CNT solution can be obtained. Meanwhile, the sheet resistance (Rs) can be measured with a 4-point probe. It was discovered that the product of m and Rs is a figure-of-merit to indicate the carbonaceous impurity level.

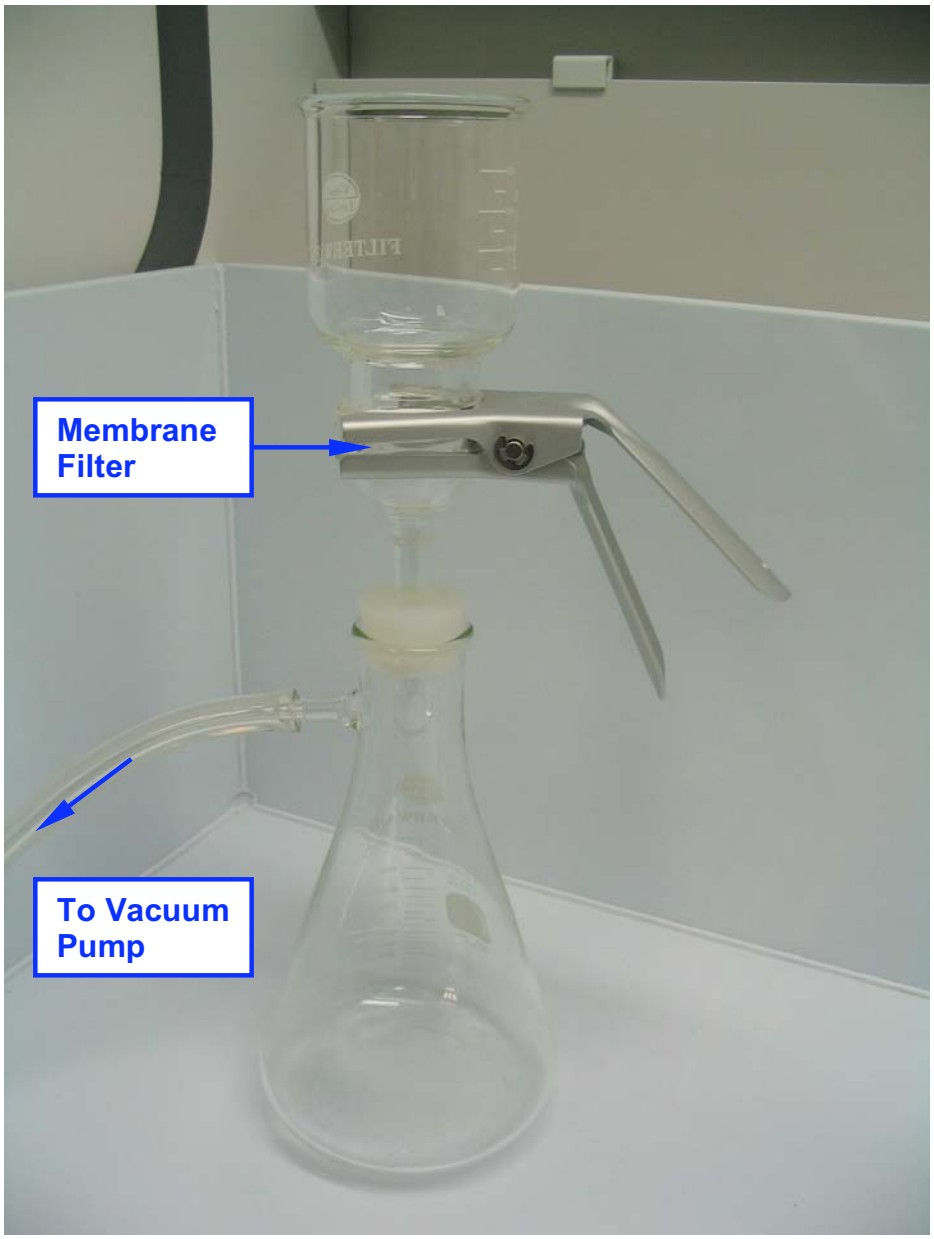

Figure 6. Assembled vacuum filtration setup

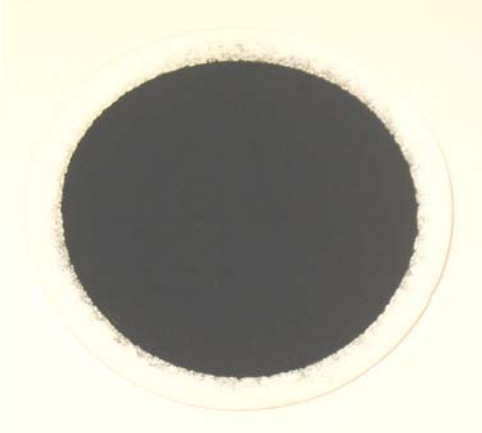

Figure 7. CNT film formed on filter disc

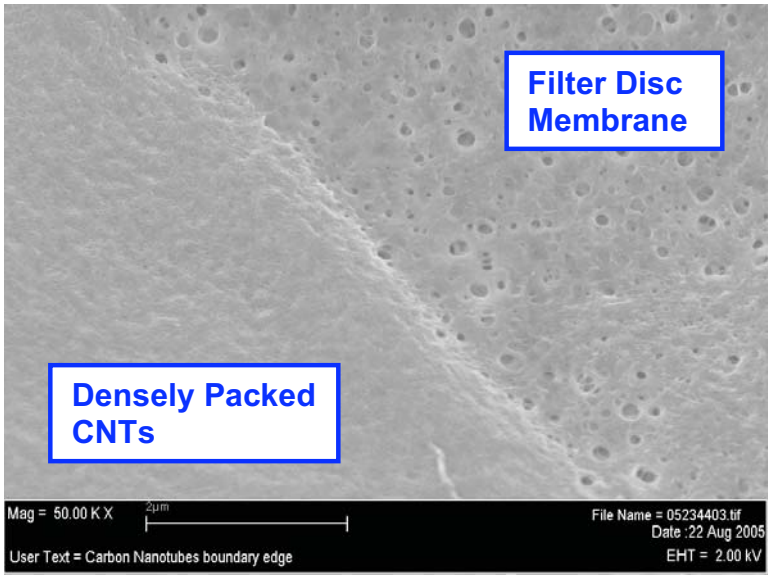

Figure 8. SEM of CNT film formed on filter disc

Raman Spectroscopy

Raman spectroscopy can provide an exceedingly powerful tool for characterizing the structures of CNTs. The resonant Raman process occurs when the transition excited by the incident laser photon energy is to a real electronic state, which can increase the signal by a factor of approximately 10^3 in comparison to the intensity in a non-resonant Raman process. Figure 9 shows the Raman setup at Brewer Science, which is equipped with a 632.8 nm He-Ne laser and a 785 nm solid-state laser. The sample preparation procedure is identical to the one used for the filter disc electrical testing. In a measured Raman spectrum, there are many features that can be identified with specific phonon modes and with specific Raman scattering processes that contribute to each feature. Particularly, the radial breathing mode (RBM) features correspond to the coherent vibration of carbon atoms in the radial direction, as if the tube were “breathing”. Such Raman features are

unique to CNTs, and occur with frequencies (ω_{RBM}) between 120 1/cm and 350 1/cm for the tubes having diameters between 0.7 nm to 2 nm. The disorder (D) mode around 1300 1/cm can come from: (1) CNT sidewall defects, (2) functional groups attached to CNT sidewall, and (3) carbonaceous impurities.

Figure 9. Raman spectroscopy measurement setup

Determination of Raw Material Source Impact

An investigation was conducted to determine the impact of two sources providing raw CNTs. These two sources are referred to hereafter as Source A and Source B. At the same time, two independent equipment sets were included in the experiment to determine the impact from the differences in the equipment set. These two equipment sets are hereafter referred to as Reactor 1 and Reactor 2. Table 2 presents the 2-factor 2-level experimental design. A replicate of each combination was included, making a total of 8 runs for this experiment.

NANOTUBE PURIFICATION RAW MATERIAL EFFECTS EXPERIMENT		
PRODUCTION FACTORS	**LEVELS**	
	(-)	(+)
Reactor	2	1
Supplier	B	A

Table 2. Experimental design to determine raw material source impact

Table 3 shows the treatment combinations and the run order. The concentration of the purified carbon nanotube solution in each sample was adjusted to OD of 1.62 at 550 nm.

-	Reactor 2	Supplier B
+	Reactor 1	Supplier A

Run Number	Treatment Combinations	Mean	Location A	Supplier B
1	4		+	+
2	2		+	-
3	1		-	-
4	4		+	+
5	3		-	+
6	2		+	-
7	3		-	+
8	1		-	-

Run Number	Treatment Combinations	Reactor	Supplier
1	4	Reactor 1	Supplier A
2	2	Reactor 1	Supplier B
3	1	Reactor 2	Supplier B
4	4	Reactor 1	Supplier A
5	3	Reactor 2	Supplier A
6	2	Reactor 1	Supplier B
7	3	Reactor 2	Supplier A
8	1	Reactor 2	Supplier B

Table 3. Treatment combinations and run order to determine raw material source impact

Investigation of Waste Stream

A sample from the aqueous waste was collected from the purification process at its most concentrated point. Similar to what is shown in Figure 6, the aqueous waste was filtered through a vacuum filtration assembly having a filter disc membrane with a nominal pore size of 0.02 μm. In this way, the solid waste materials could be collected on the filter disc. After being dried on a hotplate at 100 °C for one hour, the sample collected on the filter disc was examined with Raman spectroscopy.

RESULTS AND DISCUSSION

Screening of Raw CNTs

Metallic Impurities

XRD was conducted on three raw CNT samples that were obtained from three different vendors. The experimental results are shown, respectively, in Figure 10, which indicates the presence of Fe particles, in Figure 11, which indicates the presence of Fe and Fe_2O_3 particles, and in Figure 12, which indicates the presence of Ni particles.

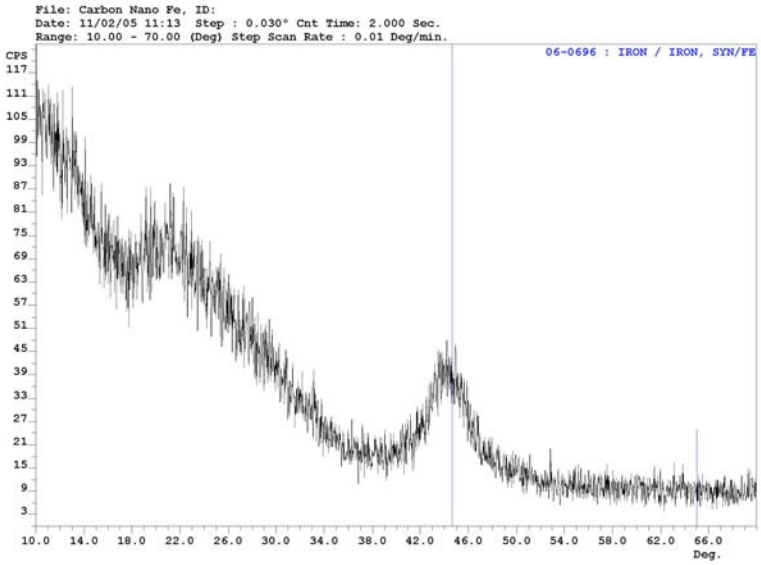

Figure 10. XRD spectrum of raw HiPco CNTs (ID: R0220) from CNI

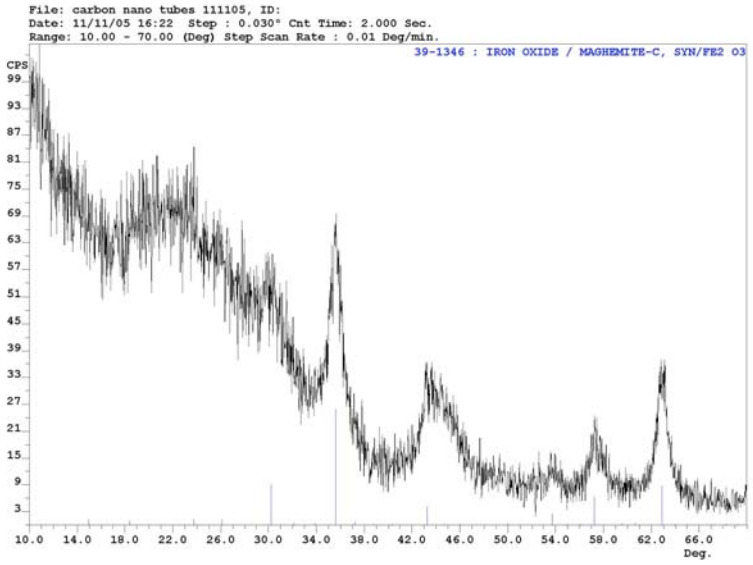

Figure 11. XRD spectrum of raw CNTs (ID: H-10-27-05) from Nano-C

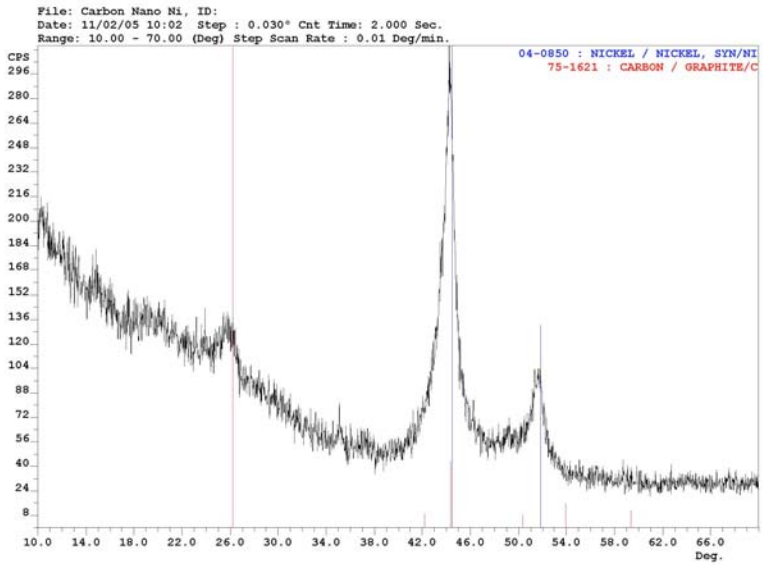

Figure 12. XRD spectrum of raw CNTs (ID: 519308) from Sigma-Aldrich

The TGA results are shown in Figure 13. Notice that all carbon materials were completely burned off at the end of the heating cycle, and only metal oxides were left as the residues. The ash content is defined as the final weight recorded by TGA, which can be used to calculate the concentrations of the metallic impurities in the original raw CNTs. The experimental results with six different raw CNT samples are summarized in Table 4.

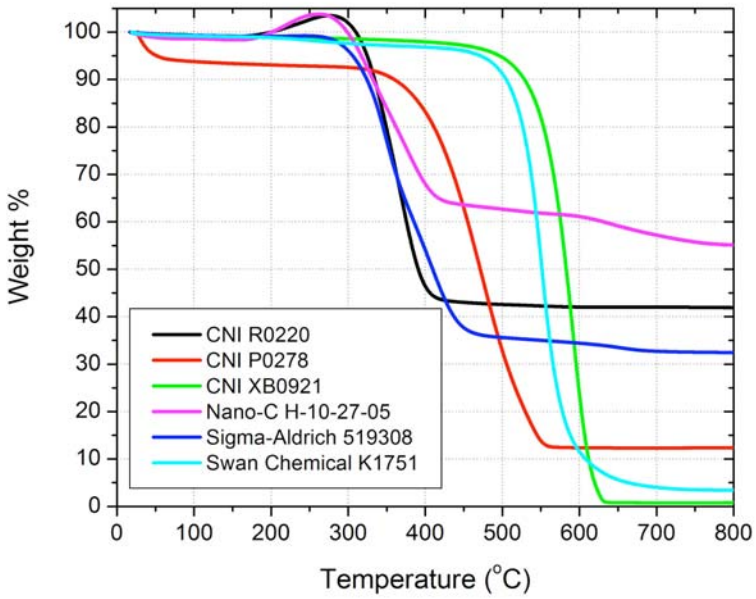

Figure 13. TGA results

Sample ID	Vendor	Ash Content
R0220	CNI	41.9%
P0278	CNI	12.3%
XB0921	CNI	0.8%
H-10-27-05	Nano-C	55.1%
519308	Sigma-Aldirch	32.4%
K1751	Swan Chemical	3.4%

Table 4. Ash contents in raw CNT samples recorded by TGA

Carbonaceous Impurities

The decanted CNT suspension was further diluted with SDS solution to various concentration levels, and then the optical absorption spectra of these samples were measured in the visible and near-infrared regions (12,500 1/cm – 25,000 1/cm) at a spectral resolution of 1 nm by using a spectrophotometer (Cary 300) in the two-beam mode. During all spectral scans, a sample of pure SDS solution was situated in the reference optical path, and thus the directly measured OD data had already excluded the absorption due to the aqueous surfactant solution. A typical optical absorption spectrum obtained in the study is shown in Figure 14 (a), which features a pronounced superposition of multiple sharp peaks originating from the optical transitions, namely S_{22} and M_{11}, in the electronic density of states (DOS) of the SWNTs and a broad baseline originating from the π-plasmon activities in both SWNTs and carbonaceous impurities. When heavy water was used instead of deionized water to prepare the surfactant solution, the sharp peaks originating from the S_{11} optical transitions were also found. The observation of a series of absorption peaks is consistent with the fact that a HiPco process usually produces SWNTs with a wide distribution of chiralities. To reveal the detailed structure, one particular absorption peak in Figure 14 (a) is enlarged and displayed in Figure 14 (b). Note that the peak structure exhibits a prominent Lorentzian line shape, as illustrated by the fitting curve in Figure 14 (b). In contrast, the optical absorption spectrum of the α-C suspension features only a broad baseline, as shown in Figure 15.

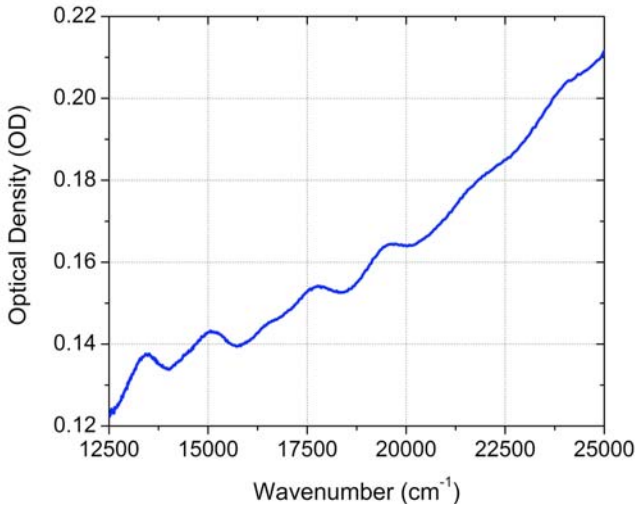

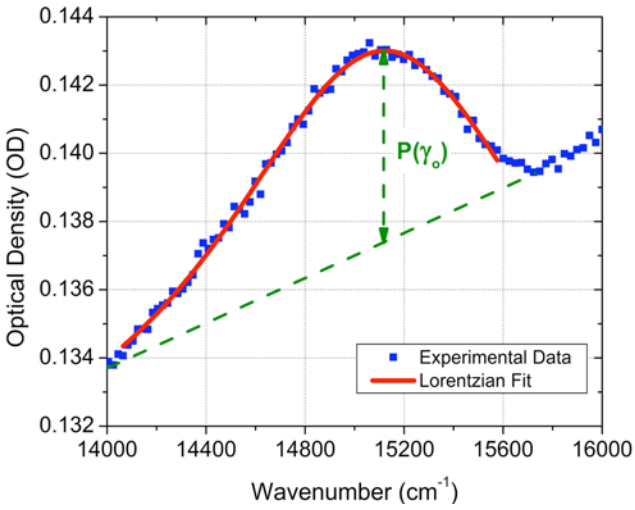

Figure 14. (a) Optical absorption spectrum of raw HiPco CNTs suspended in aqueous SDS solution (b) One enlarged spectral window of the spectrum in (a)

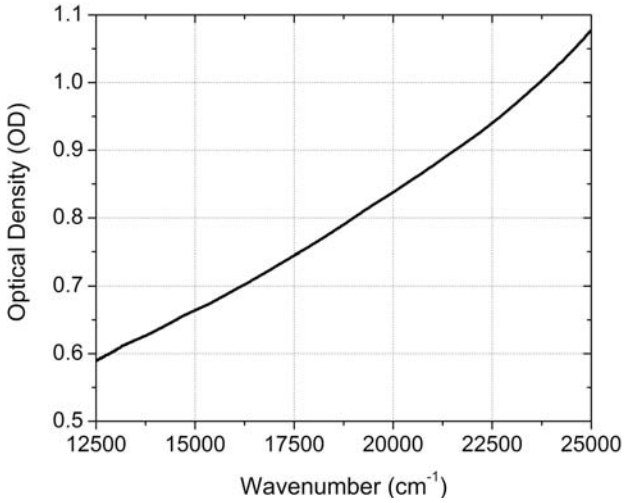

Figure 15. Optical absorption spectrum of α-C suspended in aqueous SDS solution

If the optical absorption spectrum measured from the CNT suspension can be correctly decomposed into there parts in corresponding to their physical mechanisms: (1) optical transitions in the electronic DOS of the SWNTs; (2) π-plasmon activities in the SWNTs; and (3) π-plasmon activities in the carbonaceous impurities, it would become straightforward to determine the constitution ratio of carbonaceous impurities to pristine SWNTs. As indicated in Figure 14 (b), the sharp peak in the spectrum can be easily singled out from the broad baseline. Based on optical absorption spectrum alone, however, the π- plasmon activities in the SWNTs and those in the carbonaceous impurities cannot be analytically distinguished. Furthermore, an accurate data analysis is obstructed by the lack of a SWNT reference sample in which the constitution ratio of

carbonaceous impurities to pristine SWNTs is pre-known. To address this issue, a numerical indicator was defined as a figure of merit for comparing the relative carbonaceous impurity levels among different raw CNT samples.

The spectral window ranging from wavenumber 14,000 1/cm to 16,000 1/cm, as displayed in Figure 14 (b), was selected for conducting the data analysis. The OD measured at the absorption peak (γ_o) can be expressed in terms of the concentration of pristine SWNTs (c_{SWNT}), the concentration of carbonaceous impurities (c_{CI}), the absorption coefficient of the optical transitions in the electronic DOS of the SWNTs (ϕ_P), the absorption coefficient of the π-plasmon activities in the SWNTs (ϕ_{B-SWNT}), and the absorption coefficient of the π-plasmon activities in the carbonaceous impurities (ϕ_{B-CI}) as following:

$$OD(\gamma_o) = c_{SWNT} \cdot [\phi_P(\gamma_o) + \phi_{B-SWNT}(\gamma_o)] + c_{CI} \cdot \phi_{B-CI}(\gamma_o) \quad (1)$$

Define two symbolic functions as followings:

$$\beta(\gamma_o) \equiv \phi_{B-CI}(\gamma_o)/\phi_{B-SWNT}(\gamma_o) \quad (2)$$

$$\kappa(\gamma_o) \equiv \phi_P(\gamma_o)/\phi_{B-SWNT}(\gamma_o) \quad (3)$$

By using equations (2) and (3), equation (1) can be transformed as following:

$$c_{CI}/c_{SWNT} = [\kappa(\gamma_o) \cdot \frac{OD(\gamma_o)}{c_{SWNT} \cdot \phi_P(\gamma_o)} - \kappa(\gamma_o) - 1]/\beta(\gamma_o) \quad (4)$$

In this form, the constitution ratio of carbonaceous impurities to pristine SWNTs (c_{CI}/c_{SWNT}) is explicitly expressed. Assume $c_{SWNT} \cdot \phi_P(\gamma_o)$ can be approximated by the portion of $OD(\gamma_o)$ that is labeled "$P(\gamma_o)$" in Figure 14 (b), which represents the sharp absorption peak linearly separated from the broad absorption baseline, then equation (4) becomes

$$c_{CI}/c_{SWNT} = [\kappa(\gamma_o) \cdot OD(\gamma_o)/P(\gamma_o) - \kappa(\gamma_o) - 1]/\beta(\gamma_o) \quad (5)$$

Define CIL (Carbonaceous Impurity Level) as following:

$$CIL \equiv OD(\gamma_o)/P(\gamma_o) \quad (6)$$

Note that the numerical value of CIL can be directly calculated from the measured optical absorption spectrum, and equation (5) can be rewritten in term of CIL as following:

$$c_{CI}/c_{SWNT} = [\kappa(\gamma_o) \cdot CIL - \kappa(\gamma_o) - 1]/\beta(\gamma_o) = f_M(CIL) \quad (7)$$

Although the numerical value of f_M cannot be obtained due to the lack of any quantitative information about $\beta(\gamma_o)$ and $\kappa(\gamma_o)$, the significance of equation (7) is that it manifests f_M as a monotonically increasing function of CIL. If the same experimental procedure is followed and the same spectral window is used, the variations in $\beta(\gamma_o)$ and $\kappa(\gamma_o)$ can be neglected. Thus, f_M can be simply re-scaled in term of CIL, in other words, CIL alone can be used as a figure of merit for characterizing the quality of the as-produced SWNTs, i.e. a lower CIL value represents a higher purity.

The CIL values of the prepared HiPco CNT suspensions were calculated according to equation (6) and then plotted versus the associated $OD(\gamma_o)$, as shown in Figure 16. The

average CIL value is 28.7, and the variation of CIL is less than 3%. Note that the numerical values of CIL are independent of the concentrations of the CNT suspensions. This demonstrates that the light scattering effect does not affect CIL, at least in the concentration range observed in this study.

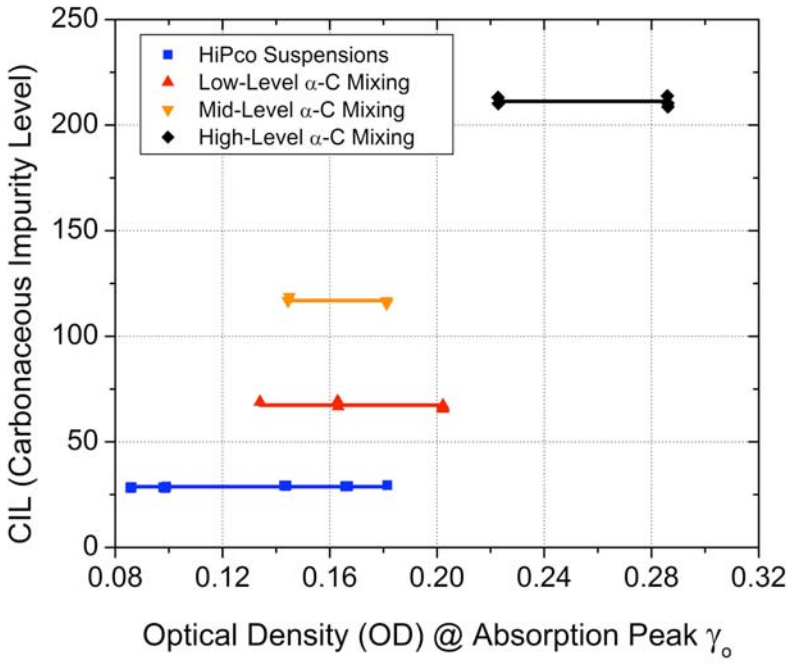

Figure 16. Calculated CIL vs. measured OD at absorption peak γ_o

Because there is no absorption peak in the spectrum of the α-C suspension, i.e., $P(\gamma_o) = 0$, as shown in Figure 15, the CIL value of this sample is infinitely large according to equation (6). Then this α-C suspension was purposely mixed with the CNT suspension. The CIL value of this "contaminated" sample was recalculated and plotted in Figure 16 as well. Note that each time when an additional amount of α-C was added into the CNT suspension, the new CIL value showed a clear jump compared with the previous level.

Higher density carbonaceous impurities and metallic nanoparticles can be slung out from lower density CNTs during an ultracentrifuge process, and thus some degree of purification can be achieved. One sample from the original HiPco CNT suspension underwent an ultracentrifuge at 120,000 g for 1 hour (Sorvall Discovery 90 SE). At the end of this treatment, a considerable amount of black substances were observed at the bottom of the solution. The upper ~ 80% portion of this purified CNT suspension was decanted out, and then a spectral study was performed by following the same procedure. As shown in Figure 17, compared with the optical absorption spectrum obtained before the ultracentrifuge, the new one exhibits a less steep baseline and a blue spectral shift. The overall absorption peak pattern is similar to the one observed before the ultracentrifuge, but contains more resolved structures, as indicated by the increasing

number of base Lorentzian functions required in order to achieve a satisfactory data fitting. These phenomena are commonly used as qualitative measures when a CNT sample of high purity is obtained. By using the directly measured spectral data in the same spectral window (14,000 1/cm – 16,000 1/cm), the CIL value of the purified CNT suspension was calculated according to equation (6), and it was found to have dropped to 11.8. Note that the effectiveness of a purification treatment by ultracentrifuge can be quantitatively characterized by the reduction of the CIL values, which is more than 58% in this case. A purification treatment by a chemical means usually attaches some functional groups to the tube sidewall. Consequently, the electronic band structures of such purified CNTs can be dramatically reshaped. Therefore, CIL alone is not sufficient for quantitatively characterizing the effectiveness of a chemical purification treatment.

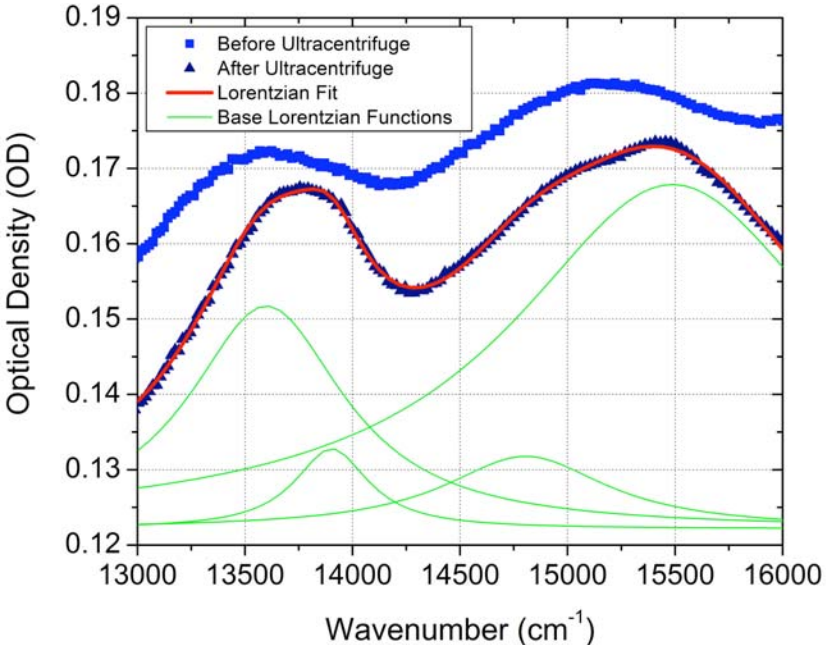

Figure 17. Effect of ultracentrifuge treatment on OD spectrum of raw HiPco CNTs suspended in aqueous SDS solution

The experimental procedure presented herein for preparing aqueous CNT suspensions is quite simple, and the major processing conditions, such as the ultrasonic power density, the sonication duration, the sediment duration after sonication, and the temperature of the CNT suspension, can all be well controlled. Therefore, it is reasonable to expect that the numerical values of CIL calculated from the optical absorption spectra of these CNT suspensions are reliable and reproducible. Optical absorption spectra can also be measured from CNT films. However, it is fairly difficult to control the thickness and uniformity of CNT films. Furthermore, there exists a polarization-dependence effect caused by the local in-plane orientation of the CNTs in the film. Due to these concerns, calculating the numerical values of CIL from the optical absorption spectra of CNT films is not recommended. The absorption peak in the spectral window (14,000 1/cm – 16,000 1/cm) selected in this study is suitable for characterizing the raw CNTs synthesized by

the HiPco process. In the case of other types of raw CNTs, different absorption peaks might be more appropriate, but the principle for conducting the data analysis can still be the same as what is outlined herein. The use of SDS in either deionized water or heavy water as the surfactant solution can reveal nearly all absorption peaks from common SWNT species with little solvent interference. Because CIL is a relative indicator of the carbonaceous impurity level, not the actual c_{CI}/c_{SWNT}, a systematic correlation between the CIL values calculated based on the absorption peaks from different SWNT species needs to be established before making any definite conclusion. By simultaneously measuring the amount of the additional α-C added into a CNT suspension and monitoring the induced increment in CIL, it is possible to gain some insights about $\beta(\gamma_o)$ and $\kappa(\gamma_o)$, and eventually to calculate the absolute numerical value of c_{CI}/c_{SWNT} according to equation (7). However, this might overestimate the actual c_{CI}/c_{SWNT} in the original raw CNTs, since an ultrasonic treatment of carbon nanotubes can produce more α-C. Nonetheless, it is important to note that CIL alone is sufficient for practical use as a figure of merit for comparing the quality of raw CNTs, i.e., a lower CIL value represents a higher purity.

Characterization of Electronic-Grade CNT Solutions

Optical Density

To determine the variability of the OD measurement, a sample was subdivided into 10 aliquots. The spectrophotometer was zeroed using DI water, and then a measurement was made. After removing the sample, the spectrophotometer was again zeroed with DI water, and then the process was repeated. A total of 10 measurements were made. The standard deviation for this measurement was found to be 0.44%, as shown in Table 5.

Measurement	OD
1	2.355
2	2.378
3	2.378
4	2.363
5	2.366
6	2.344
7	2.363
8	2.36
9	2.355
10	2.363
Average	2.3625
St dev	0.010298328
% Stdev	0.44%

Table 5. Variability of OD measurement

Dilution Curve

By using the OD measurement to adjust the solution concentration has been studied on a large number of batches. As shown in Figure 18, the % error has been calculated for each dilution effort by comparing the difference between the predicted OD based on the dilution curve and the measurement of the diluted outcome. This method is therefore demonstrated to predict the diluted concentration to within ± 2.7%.

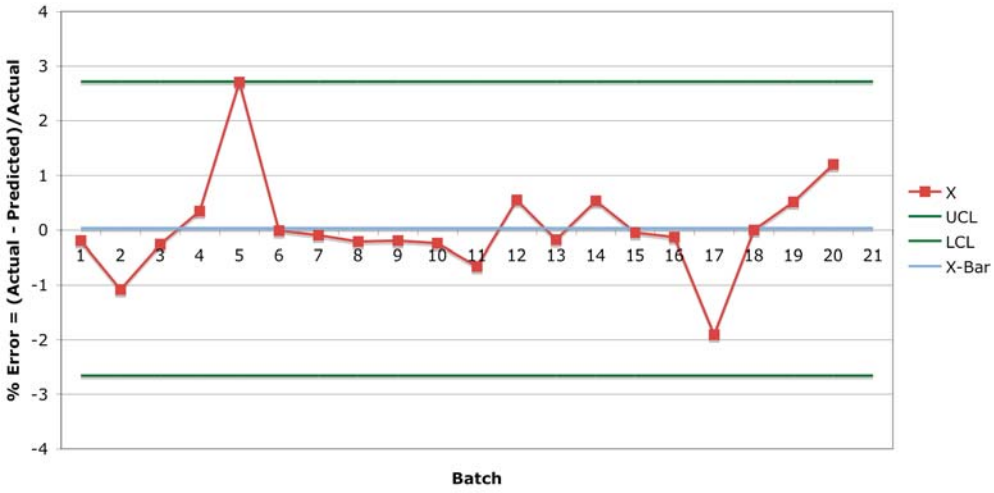

Figure 18. OD dilution curve error

Trace Metals

Consistent control of trace metals has been achieved, as shown in Figure 19.

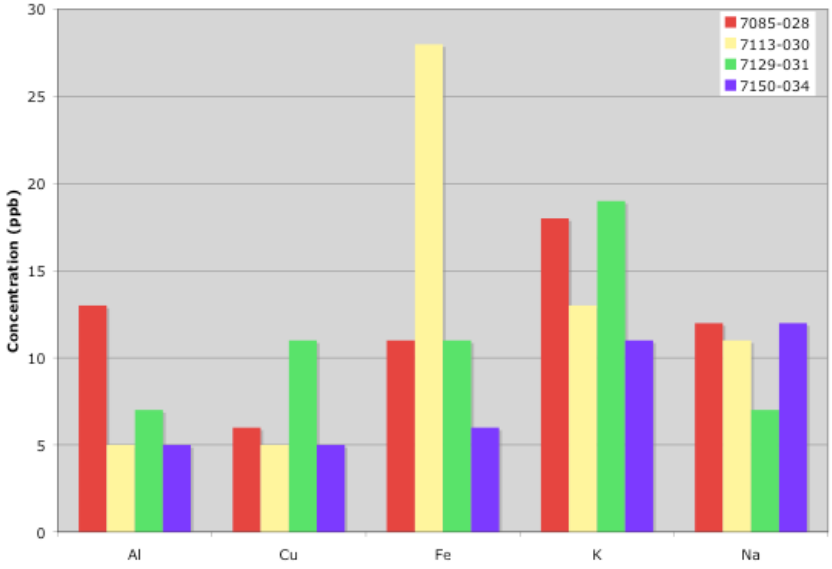

Figure 19. Consistent control of trace metals

Wafer Electrical Testing

To determine the variability of this test, a single batch of solution was subdivided into 15 mL aliquots for weekly testing. The average resistance was recorded for a period of 16 weeks. The results are shown below in Figure 20. Over the 16-week period, the standard deviation is 54%. The causes of the variation have not been determined. However, this test is not suited for measurement of product stability for the commercial application.

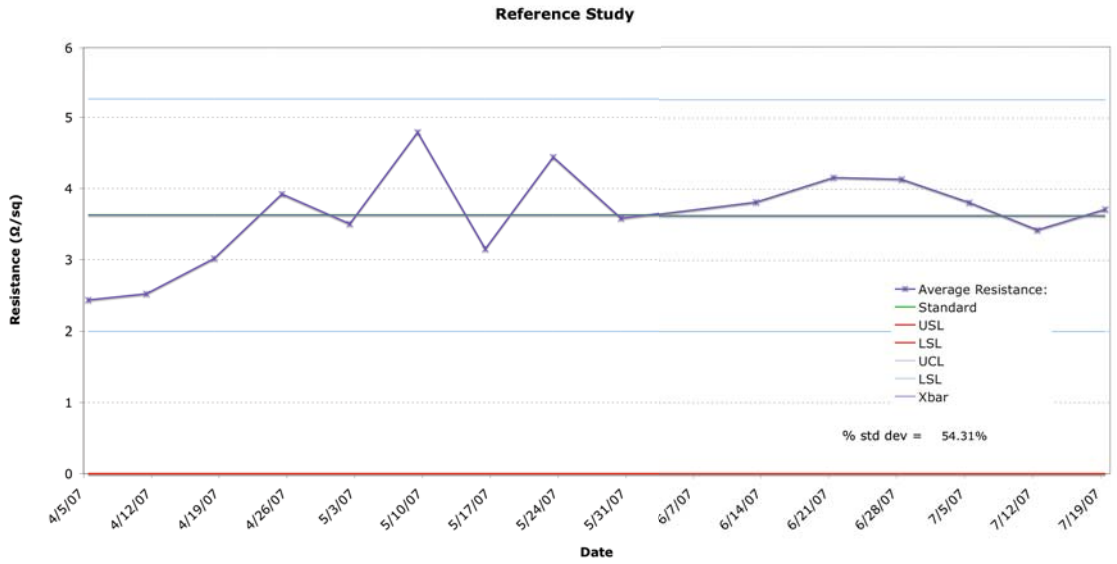

Figure 20. Variability of wafer electrical testing

Filter Disc Electrical Testing

The weight (m) and the sheet resistance (Rs) of the obtained CNT film on the filter disc membrane can be expressed in the following forms:

$$m = \rho_m \cdot A \cdot t \quad (8)$$

$$Rs = \rho / t \quad (9)$$

where ρ_m is the mass density of the CNT film, A is the area of the CNT film, t is the thickness of the CNT film, and ρ is the resistivity of the CNT film. Multiplying equation (8) and (9) gives the following form:

$$m \cdot Rs = \rho_m \cdot A \cdot \rho \quad (10)$$

Beyond the percolation threshold, ρ_m becomes a constant. The variation of the area of the CNT film is negligible. Therefore, $m \cdot Rs$ is directly proportional to ρ, which can reflect the level of carbonaceous impurities in the raw CNTs.

Raman Spectroscopy

The typical Raman spectra obtained at excitation 632.8 nm and 785 nm are shown in Figure 21 and 22, respectively.

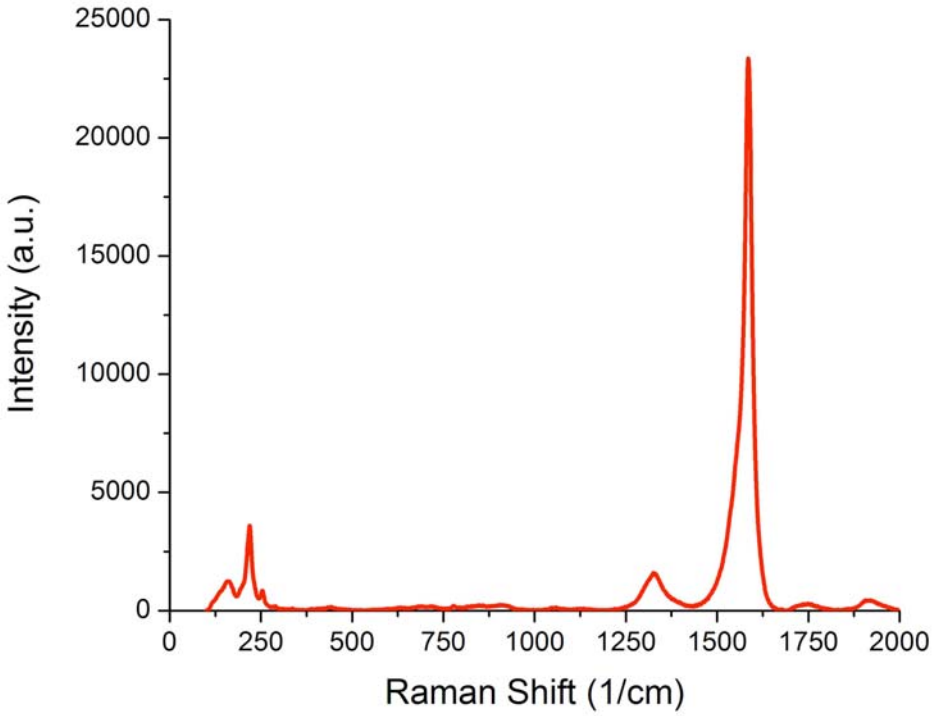

Figure 21. Typical Raman spectrum obtained at excitation 632.8 nm

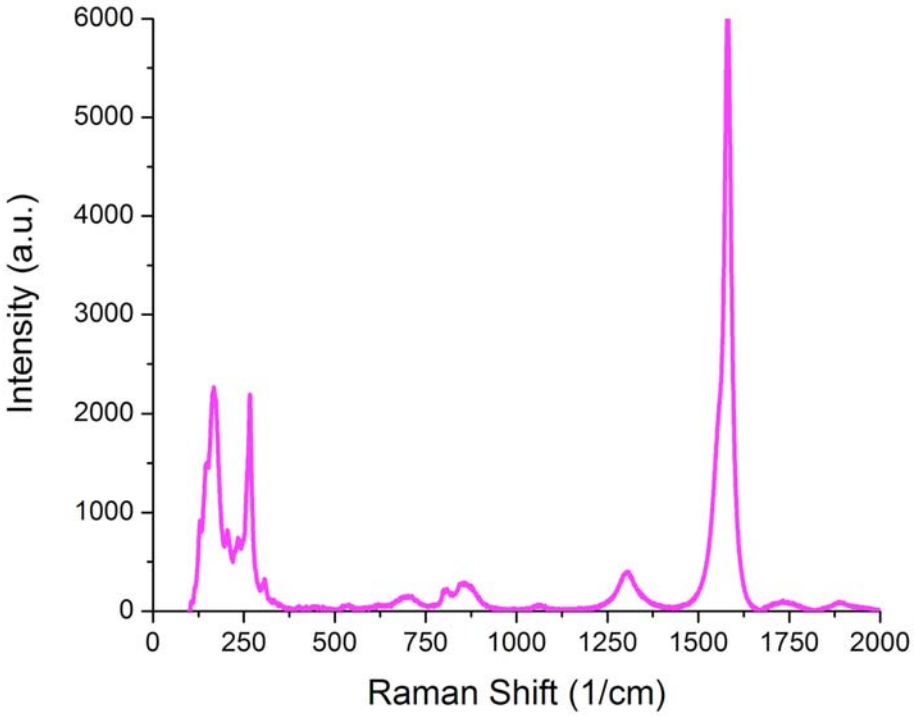

Figure 22. Typical Raman spectrum obtained at excitation 785 nm

Determination of Raw Material Source Impact

Figure 23 shows the statistical analysis on the obtained sheet resistance data, which demonstrate that the sheet resistance of the carbon nanotube layer spin-coated on the silicon oxide wafer is significantly different between the two raw material sources. The carbon nanotubes from Supplier B exhibited sheet resistance values twice as high as those from Supplier A. In contrast, the reactor set did not exhibit significant effect. There was no interactive effect between the reactor set and the raw material source.

Location	Location	Supplier	UCL
-	4.40375	6.04	
+	4.655	3.01875	
Effect	0.25125	3.02125	1.2572296

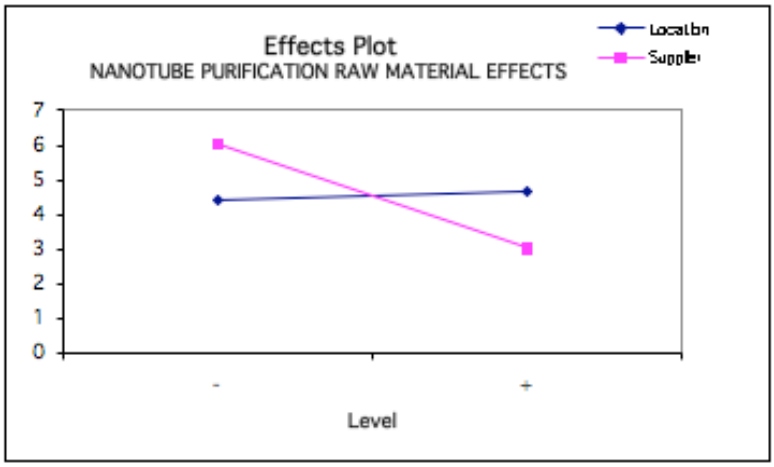

Factor	Effect	UCL
Location	0.25125	1.2572296
Supplier	3.02125	1.2572296
Interaction	0.32875	1.2572296

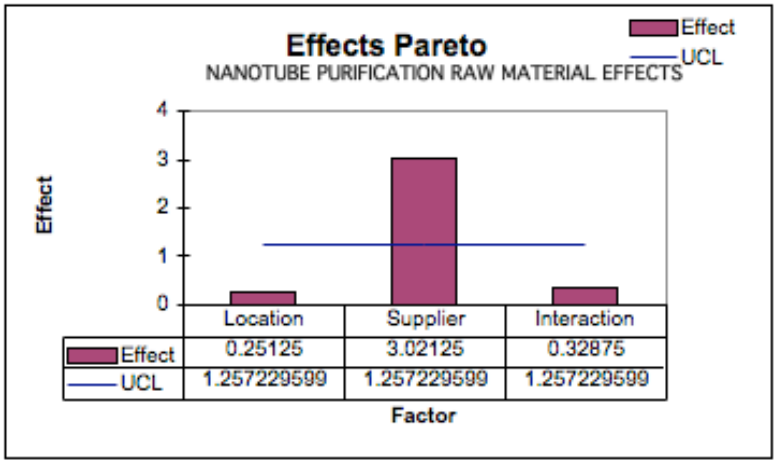

Figure 23. Raw material source impact indicated by sheet resistance measurement

As shown in Figure 24, there was a significant difference in $m \cdot Rs$ between the two suppliers. In contrast, there was no significant difference between the reactor sets.

Location	Location	Supplier	UCL
-	1.48075	1.734	
+	1.4275	1.17425	
Effect	0.05325	0.55975	0.49724625

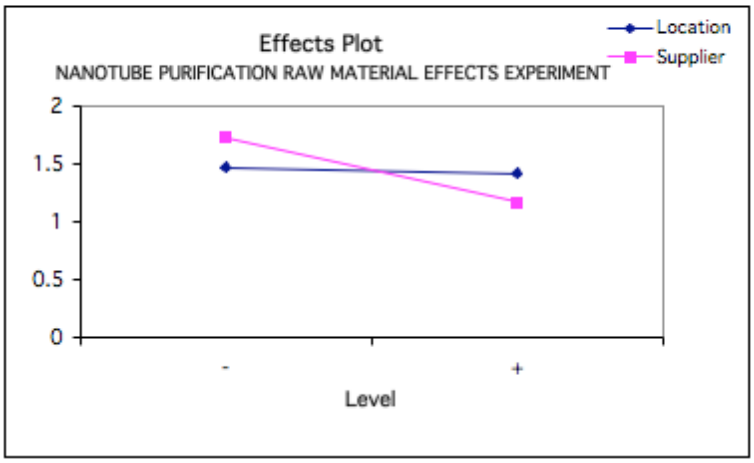

Factor	Effect	UCL
Location	0.05325	0.49724625
Supplier	0.55975	0.49724625
Interaction	0.21125	0.49724625

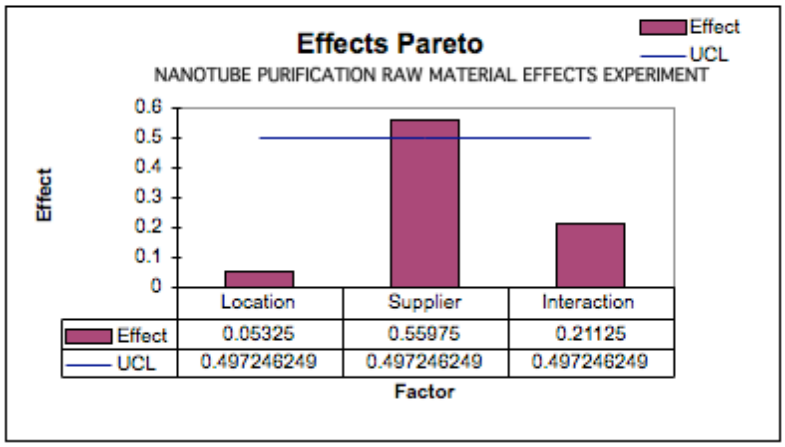

Figure 24. Raw material source impact indicated by measurement of $m \cdot Rs$

The trace metal levels measured with ICP-MS are shown in Table 6. Note that two samples are unusually high in iron and significantly higher levels of iron in the samples produced in Reactor 2 from Supplier A.

	Reactor 2 (Supplier A)	Reactor 2 (Supplier B)	Reactor 2 (Supplier B)	Reactor 2 (Supplier A)	Reactor 1 (Supplier B)	Reactor 1 (Supplier B)	Reactor 1 (Supplier A)	Reactor 1 (Supplier A)
Na	17.87	21.04	0	56.57	64.47	14.67	99.77	12.33
Mg	0	0	0		0	0	0	0
Al	0	0	0	0	0	0	0	0
K	3.7	2.39	0	1.17	1.07	0	48.86	2.88
Ca	41.79	29.9	17.39	33.54	17.27	15.95	29.57	19.89
Cr	0	0	0		0	0	0	0
Mn	0	0	0		0	0	0	0
Fe	415.77	7.93	0.76	687.42	0	0	0	0
Cu	0	0	5.17	0	0	0	0	0

Table 6. Trace metals in CNT solutions purified from two sources of raw CNTs

Figure 25 shows the typical Raman spectra of the samples. There are two distinctive peaks: the Graphite, or "G" mode, peak is located near 1600 1/cm, and the Disorder, or "D" mode, peak near 1300 1/cm. The area ratio of these two peaks indicates the degree of orderliness of the carbon nanotube structure, with a higher G/D area ratio indicating less carbonaceous impurities.

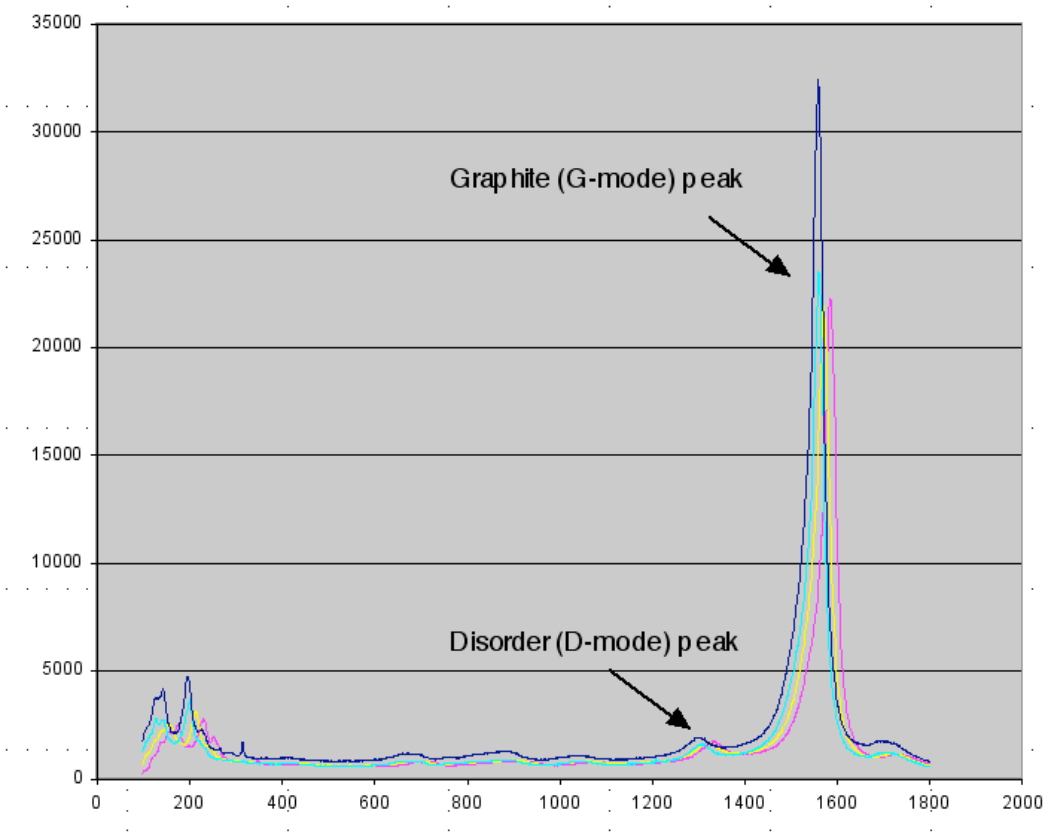

Figure 25. Raw material source impact indicated by Raman measurement

As shown in Figure 26, both the raw material source and the reactor set have significant impacts on the G/D Area ratio. The reactor sets responded inversely to the raw material sources.

Location	Reactor	Supplier	UCL
-	32.455	16.3085	
+	12.05975	28.20625	
Effect	20.39525	11.89775	7.85562218

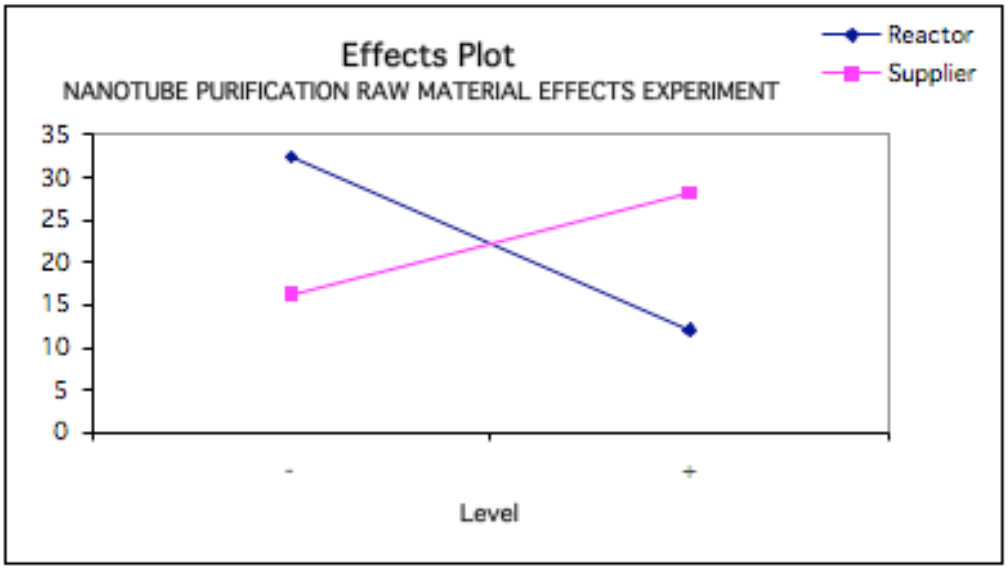

Factor	Effect	UCL
Reactor	20.39525	7.85562218
Supplier	11.89775	7.85562218
Interaction	12.03325	7.85562218

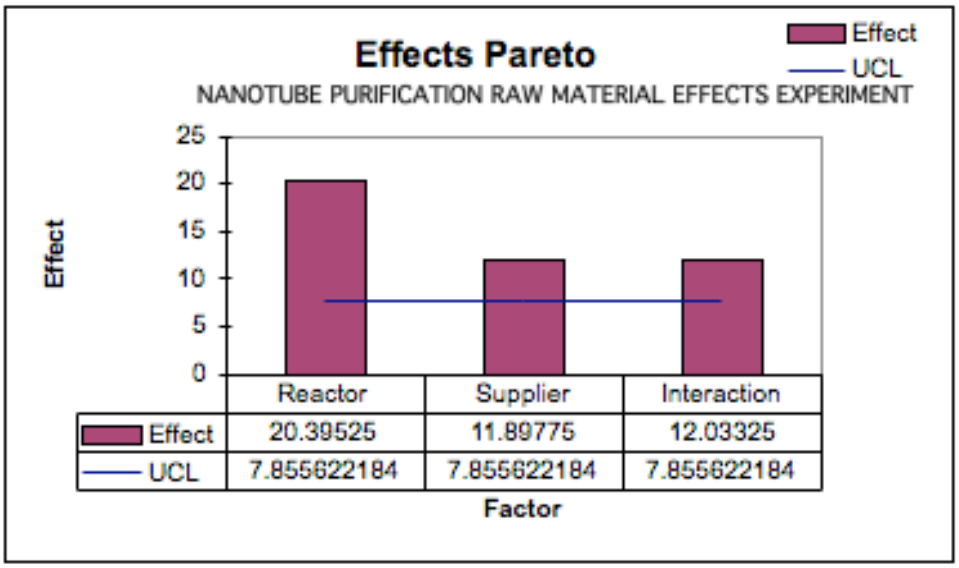

Figure 26. Raw material source impact indicated by G/D area ratio measurement

Investigation of Waste Stream

The Raman spectrum measured from the waste sample collected on the filter disc shows the signature peaks of carbon nanotubes, as shown in Figure 27. These peaks include a "G-mode" peak near 1600 1/cm, a "D-mode" peak near 1300 1/cm, and a "Radial Breathing Mode" peak near 200 1/cm.

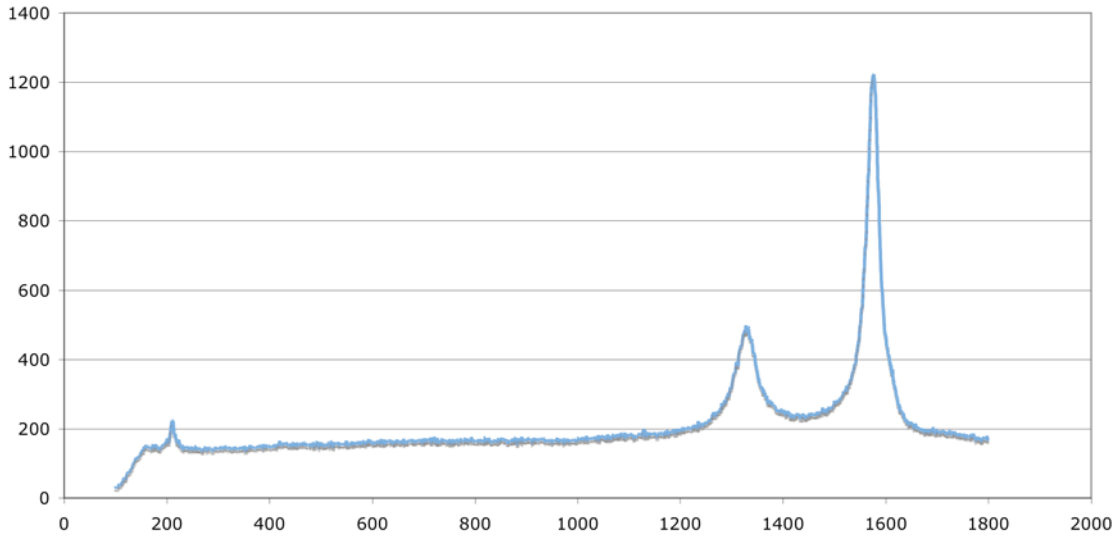

Figure 27. Raman spectrum measured from waste

CONCLUSIONS

The purification process developed at Brewer Science has been proved to be effective, reliable, and repeatable, based on the various experimental data obtained from a series of validated characterization methods.

The investigation of raw material source impact showed that the raw CNTs from the two sources react differently in the process.

The evidence that CNTs are present in the aqueous waste was found. Therefore, the aqueous waster should be segregated and collected as hazardous, until the health and environmental hazards are determined or until the purification procedure can be adjusted to exclude carbon nanotubes from the waste stream.